Chapter 10
Integration of Green Energy into Power Distribution Systems: Study of Impacts and Development of Control Methodology

N. K. Roy and H. R. Pota

Abstract Distributed generation (DG) is gaining popularity as it has a positive environmental impact and the capability to reduce high transmission costs and power losses. Although the integration of renewable energy-based DG will help reduce greenhouse gas emissions, it will rely heavily on new ways of managing system complexity. As traditional distribution networks were not designed to accommodate power generation facilities, various technical issues arise in the integration of distributed energy resources (DERs) into grids. This chapter presents an analysis of the major obstacles to the integration of green energy into power distribution systems (PDSs). Static and dynamic analyses are carried out with solar photovoltaic (PV) generators connected to different test systems to gain a clear understanding of the effect of PVs in PDSs. The results are compared with the existing utility standards to determine the critical issues in the integration of PVs into PDSs. A novel H_∞ based control methodology is proposed to ensure grid code-compatible performances of PV generators. During the controller design, special attention is given to the dynamics of the load compositions of distribution systems. It is found that the proposed controller enhances the voltage stability of distribution systems under varying operating conditions.

Keywords Composite loads · Distributed generation · D-STATCOM · Voltage stability · Photovoltaic generator · Robust control and uncertainty

N. K. Roy (✉) · H. R. Pota
School of Engineering and Information Technology, The University of New South Wales, PO Box 7916, Canberra, ACT 2610, Australia
e-mail: n.roy@student.unsw.edu.au

H. R. Pota
e-mail: h.pota@adfa.edu.au

J. Hossain and A. Mahmud (eds.), *Renewable Energy Integration*, Green Energy and Technology, DOI: 10.1007/978-981-4585-27-9_10,

10.1 Introduction

Power supply reliability, efficiency and sustainability are the major concerns in the development of future energy systems. Many countries of the world have set their targets for power generation from green energy to reduce greenhouse gas emissions, as shown in Table 10.1 [1]. To reach the goal of green energy, distributed generation (DG) is a promising option and, therefore, is receiving a great deal of interest.

Photovoltaic (PV) and wind energy-based systems are the most important green energy resources. Research on the integration of solar PV in distribution systems is still in its infancy. At present, the main concerns about high penetration levels of solar PV generation in a distribution system are the effects of intermittency on the system protection when multiple sources are connected to a radial feeder or network [2, 3]. Close attention has been paid to modeling generators and their associated controls, and distribution system equipment. A model of a PV array is proposed in [4] which uses theoretical and empirical equations, together with data provided by the manufacturer, solar radiation, cell temperature and other variables, to predict the current–voltage curve. To study interactions of PV generators within the power system, a model of PV generator developed based on experimental results [5] suggests that the maximum power point tracking (MPPT) part of the control system of a PV generator dominates the dynamic behavior of the system. A mathematical model suitable for stability analysis that includes the nonlinear behavior of grid-connected PV modules is presented in [6]. Simulations which include the entire power converter are performed in [6] to support the mathematical analysis and it is concluded that the system is more susceptible to instability under high loading levels, i.e., when operating close to its maximum power point.

Grid integration of solar PV systems is gaining more interest than traditional stand-alone systems because of the following benefits:

- under favorable conditions, a grid-connected PV system supplies the excess power, beyond the consumption required by the connected load, to the utility grid;
- it is comparatively easy to install as it does not require a battery system because the grid is used as a backup;
- no storage losses are incurred; and
- it has potential cost advantages.

It is expected that grid-connected PV systems in medium-voltage networks will be commercially accepted in the near future [7]. Therefore, it is necessary to accurately predict the dynamic performance of three-phase grid-connected PV systems under different operating conditions in order to make a sound decision on the ancillary services that need to be provided to utilize their maximum benefits without violating grid constraints. Thus, the spread and growth of solar and other distributed renewable energy has led to significant modeling and engineering analyses of distribution systems. Although DG has several potential benefits, the

Table 10.1 Renewable energy targets in different countries

Country	Target (%)	Year
Australia	20	2020
Austria	34	2020
Belgium	13	2020
China	15	2020
Denmark	30	2025
Finland	38	2020
France	23	2020
Germany	18	2020
Netherlands	14	2020
New Zealand	90	2025
Spain	20	2020
Sweden	49	2020
UK	15	2020
US	25	2025

connection of it in the existing distribution network will increase the fault level of the system. The impact of DG on the local voltage level can be significant during a contingency. Typical contingencies on a distribution network can occur in the form of single or multiple outages, such as unplanned losses of generators or distribution feeders. Several internal and external causes are responsible for equipment outages [8]. The internal causes arise from phenomena, such as insulation breakdown, over-temperature relay action or simply incorrect operation of relays. The external causes result from some environmental effects, such as lightning, high winds and icy conditions or non-weather related events, such as a vehicle or aircraft coming into contact with equipment or even human or animal direct contact. These contingencies can result in partial or full power outage in a distribution network unless an appropriate control action is taken.

A higher PV penetration level could possibly cause instability problems when a large percentage of the system load is supplied by PVs. Therefore, it is becoming more important to understand the behavior of a DG-integrated system under disturbances with practical distribution network loads since variations in loads physically close to generators are a large fraction of the generation. A practical system load is a combination of various types of loads and it is referred to as a composite load. The accurate modeling of loads is a difficult task due to several factors, such as [9]:

- large number of diverse load components;
- ownership and location of load devices in customer facilities not directly accessible to the electric utility;
- changing load composition with time of day and week, seasons, weather and through time;
- lack of precise information on the composition of the load; and
- uncertainties regarding the characteristics of many load components, particularly for large voltage or frequency variations.

Table 10.2 Interconnection system response to abnormal voltages

Voltage range (pu)	Clearing time (s)
$V < 0.5$	0.16
$0.5 \leq V < 0.88$	2.00
$1.1 < V < 1.2$	1.00
$V \geq 1.2$	0.16

Load modeling is qualitatively different from generator modeling in many aspects. Generally, only the aggregate behavior of load is required for power system stability studies rather than a whole collection of individual component behaviors [10, 11]. Thus, one cannot escape the necessity to analyze the impact of bus load compositions in the distribution system behavior.

It is known that the majority (more than 60 %) of power system loads are induction motors, the impact of which must be taken into account during network analysis [12]. A higher proportion of induction motors in the composite loads could cause voltage stability problem which could disconnect DG units from the network as per the current utility practice [13, 14] which demands that a system voltage should recover to an acceptable level after a disturbance within the time indicated in Table 10.2. The unnecessary disconnection of generators reduces the expected benefits of DG and should be avoided because of the increasing importance of DG. In this context, it is particularly important to supply reactive power to the dynamic load to maintain system stability, thereby keeping DG units connected.

Although inverter-connected PV systems have their own reactive power capability, they are not allowed to operate in voltage control mode to avoid controller interactions [13, 14]. Moreover, in order to contribute more real power into a system, small-scale PV units are operated at unity power factor (pf) [15]. It is not advised to use PV inverters with a variable pf because, at high penetration levels, this may increase the number of balanced conditions of load demands and generations and, subsequently, increase the probability of islanding which is a safety hazard [7]. If DG units are not allowed to regulate voltage, additional sources of reactive power need to be installed at critical locations to supply the reactive power of a system.

It is well-known that a static synchronous compensator (STATCOM) has excellent performance in terms of its response speed and capabilities to reduce system power loss and harmonics, improve voltage level and stability, and decrease occupation area [16, 17]. The internal controls of a Distribution STATCOM (D-STATCOM) play a very important role in maintaining the system voltage. The use of suitable control methods in a D-STATCOM may offer a better performance along with making possible tracking of the desirable references more efficiently. Conventional controllers for D-STATCOMs are mainly PI controllers [18, 19], the tuning of which is a complex task for a nonlinear system with switching devices. To avoid the limitations of PI controllers, a linear quadratic regulator (LQR) method is used in [20] to design a STATCOM controller which

has a superior performance. Compared to the LQR method [20], which uses states as feedback, linear quadratic Gaussian (LQG) controller is more realistic as it can be designed using only measurable outputs and state variables estimated from them [21]. However, linear controllers designed based on the given operating point are not suitable in the event of large variations in the system model. To improve the performance of an LQG controller, model mismatches or uncertainties can be bounded by an H_∞ norm which provides robust closed-loop stability as well as optimal performance [22]. As distribution networks have different types of loads, a controller designed without regard to a tight bound on variations in load compositions will not lead to a satisfactory performance. However, this important issue has not been considered in the existing literature. The superior dynamic performance of the D-STATCOM compared to many other compensating devices encourages further refining its control scheme to achieve robust performance without enhancing its reactive power capacity.

This chapter makes three contributions: (a) an investigation of the static voltage stability of distribution networks through Q–V analysis for different contingencies; (b) an examination of the impact of different load compositions on the dynamic behavior of distribution networks; and (c) a novel D-STATCOM controller design which is robust to variations in load compositions in a practical distribution system.

The organization of this chapter is as follows. Section 10.2 presents the static voltage stability analysis of the system. The mathematical model of the system for dynamic simulation is described in Sect. 10.3. Section 10.4 demonstrates the impact of various load compositions on the distribution system. The controller design is given in Sect. 10.5 and the performance of the designed controller is evaluated for different operating conditions in Sect. 10.6. Concluding remarks are given in Sect. 10.7.

10.2 Static Voltage Stability Analysis

A 16-bus 3-feeder distribution test system [23], as shown in Fig. 10.1, is used in this study. Two PV generators, one at bus 2 and one at bus 3, are connected to the distribution system. The total load on the system is 28.7 MW, 17.3 MVAr. The test system data with distributions of system loads in different nodes is given in Appendix-I. The PV system used in this analysis is operated at unity pf to comply with the grid code requirement [13].

According to the Q–V method [12], the bus voltage magnitude (V) increases as the reactive power (Q) injection at the same bus is increased. When the voltage of any bus decreases with an increase in the Q for that bus, the system is said to be unstable. The reactive power margin (Q-margin) is measured as the distance between the lowest MVAr point of the Q–V curve and the voltage axis, as shown in Fig. 10.2 [24]. Based on the Q–V analysis, the impacts of high PV penetration and the behavior of the system under contingencies are described below.

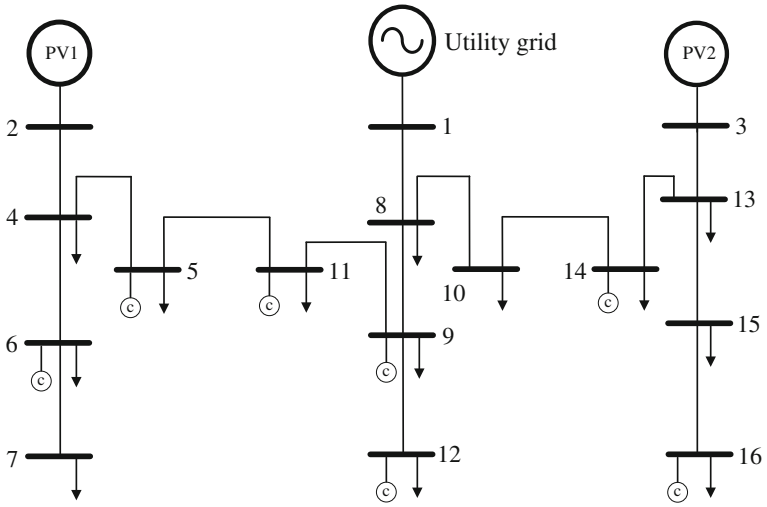

Fig. 10.1 Single *line* diagram of 16-bus distribution test system

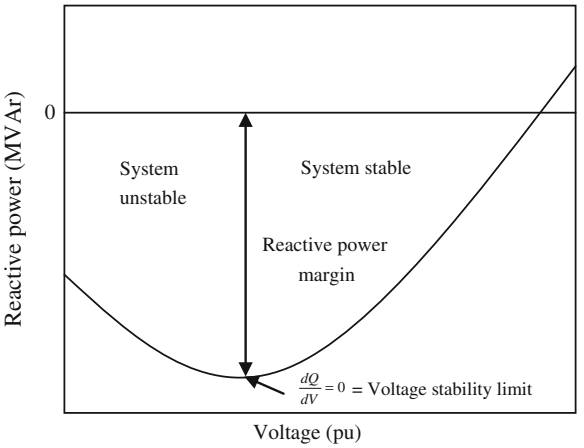

Fig. 10.2 Typical reactive power-voltage (Q–V) *curve*

10.2.1 Impact of High PV Penetration

The penetration level of PV (%PV penetration) is given by

$$\%\ \text{PV penetration} = \frac{P_{\text{PV}}}{P_{\text{load}}} \times 100 \tag{10.1}$$

where P_{PV} is the total power delivered by the PV generator and P_{load} is the peak load demand.

Table 10.3 Q-margins (MVAr) for different PV penetration levels

Bus no.	Penetration level				
	20 %	40 %	60 %	80 %	100 %
2	29.80	31.07	32.19	33.18	34.06
3	37.78	39.17	40.42	41.55	42.57
4	35.59	36.93	38.04	38.99	39.80
5	46.21	47.69	48.89	49.88	50.69
6	26.43	27.56	28.57	29.46	30.28
7	24.77	25.85	26.82	27.69	28.49
8	167.60	169.96	171.62	172.74	173.42
9	82.43	84.25	85.65	86.73	87.55
10	82.07	83.97	85.55	86.85	87.92
11	52.46	53.99	55.22	56.21	57.02
12	55.12	56.52	57.73	58.83	59.79
13	48.45	49.89	51.13	52.21	53.14
14	69.37	71.12	72.58	73.80	74.82
15	37.95	39.21	40.34	41.37	42.32
16	34.97	36.15	37.23	38.22	39.13

The Q-margins of the system for increasing PV penetration levels are shown in Table 10.3 which signify that PV generators have positive impacts on the system's Q-margin. In this scenario, the generations at both the PV buses are increased by the same amount. As the penetration level of PV increases, static voltage stability of the system also increases.

10.2.2 Behavior of System Under Contingencies

To get an idea of the system's vulnerability, Q–V analysis is performed when PV units are tripped as a result of disturbances in the system. Before application of the contingency, it is assumed that PV1 and PV2 are supporting the total system load equally. Figure 10.3 shows the Q-margins of the load buses when PV generators are tripped from the system. It can be seen that the tripping of multiple PV generators reduces the system stability compared to the tripping of a single PV generator.

It is expected that the penetration level of grid-connected distributed energy resources (DERs) will increase substantially over the next few decades. With the increased penetration of DG, tripping of massive generation due to local disturbances can further risk the stability of the whole system.

The most common operational problems in distribution systems are the overloads due to high demand in peak hours and inadequate voltage levels at system buses. Load change exceeding the normal boundary can overload the lines and transformers which is a safety hazard. To investigate the effect of overloading, it is considered that initially, PV1 and PV2 are equally supporting the nominal system load and then loading of the system is increased keeping the penetration level of

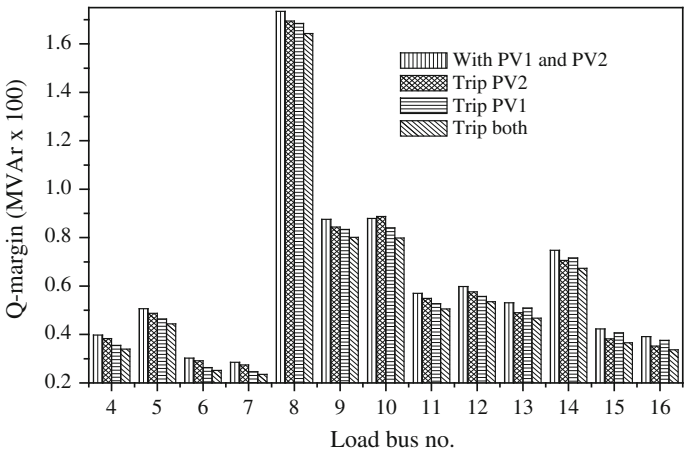

Fig. 10.3 Q-margins of load buses under contingencies

Table 10.4 Q-margins of load buses before and after contingency

Load bus no.	Q-margin (MVAr)			
	No contingency	20 % overload	30 % overload	Outage of line 2–4 and 30 % overload
4	39.80	37.41	36.22	31.56
5	50.69	47.85	46.44	41.65
6	30.28	28.40	27.45	23.19
7	28.49	26.71	25.80	21.70
8	173.42	168.49	166.05	160.71
9	87.55	83.76	81.89	77.13
10	87.92	84.68	83.01	78.78
11	57.02	53.99	52.48	47.73
12	59.79	56.93	55.50	51.11
13	53.14	51.04	49.97	47.54
14	74.82	72.00	70.56	66.93
15	42.32	40.60	39.73	37.90
16	39.13	37.53	36.72	35.05

PV generators same. The effect of overloading of the system is tabulated in Table 10.4 from which it can be investigated that a sudden overloading reduces the voltage stability of the system. The impact of multiple contingencies is more severe than a single contingency in a distribution network. Sudden outage of a line and growth in demand significantly reduces the system's stability margin, as depicted in Table 10.4.

In this study, contingency analysis is carried out using a steady-state or power flow model of the distribution system. Dynamic stability assessment is described in the next section.

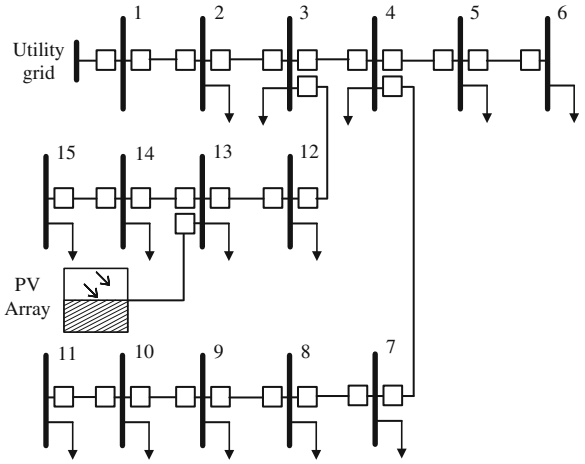

Fig. 10.4 Single *line* diagram of Kumamoto 15-bus distribution system

10.3 System Model for Dynamic Analysis

To investigate the dynamic behavior of system, a Japanese practical distribution system shown in Fig. 10.4 is considered [25]. A PV generator is connected at bus 13 and bus 1 is connected to the utility grid. The total load on the system is 6.301 MW, 0.446 MVAr. The PV generator has the capability to support 50 % of the system load and the rest is supplied by the grid. The test system data with loads is given in Appendix-I.

10.3.1 Solar PV

A PV generator consists of arrays of solar PV modules. PV modules produce DC power which is converted into AC power by an inverter. It is essential to create aggregate equivalent generators instead of modeling each individual inverter. Small-scale PV generators are typically aggregated at the distribution interface buses. Figure 10.5 shows a PV system connected to the grid through a DC–DC converter and a DC-AC inverter. The equivalent circuit of a PV system is shown in Fig. 10.6. The dynamics of the PV generator can be described by the following equations [6, 26].

$$\frac{di_{\mathrm{pv}}}{dt} = \frac{1}{\vartheta L_{\mathrm{pv}}} \ln\left(\frac{I_L - i_{\mathrm{pv}} - \frac{v_{\mathrm{pv}} + R_s i_{\mathrm{pv}}}{R_{\mathrm{sh}}}}{I_s} + 1\right) - \frac{1}{L_{\mathrm{pv}}}\left(v_{\mathrm{pv}} + R_s i_{\mathrm{pv}}\right) \tag{10.2}$$

$$\frac{dv_{\mathrm{pv}}}{dt} = \frac{1}{C_{\mathrm{pv}}}\left[i_{\mathrm{pv}} - N i_{\mathrm{dc}}\right] \tag{10.3}$$

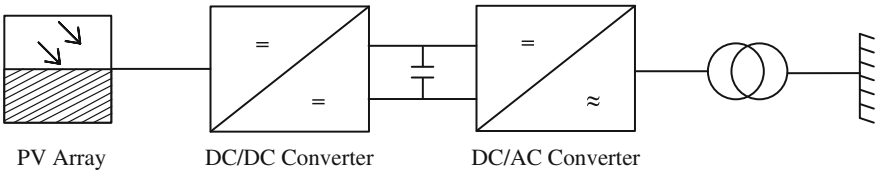

Fig. 10.5 Grid-connected PV generator

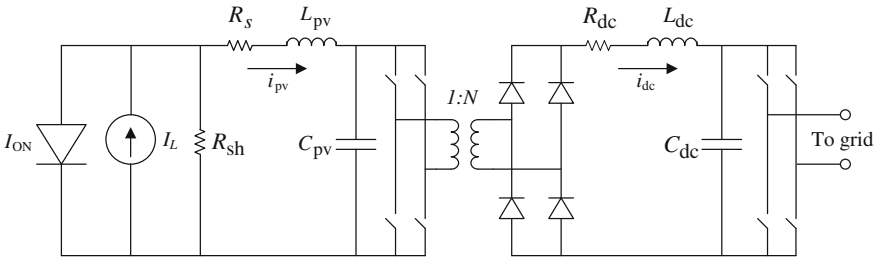

Fig. 10.6 Equivalent model of grid-connected PV generator

$$\frac{di_{dc}}{dt} = \frac{1}{L_{dc}}[Nv_{pv} - R_{dc}i_{dc} - v_{dc}] \tag{10.4}$$

$$\frac{dv_{dc}}{dt} = \frac{1}{v_{dc}C_{dc}}[P_{pv} - P] \tag{10.5}$$

where $\vartheta = \frac{q}{nskT}$, $k = 1.3807 \times 10^{-23}$ JK^{-1} is the Boltzmann's constant, $q = 1.6022 \times 10^{-19}$ C is the charge of electron, $T = 298$ K is the cell temperature and ns is the number of series cells in the PV array, I_L is the light-generated current, I_{ON} is the dark diode characteristics of photocells, L_{pv} and C_{pv} is the wiring inductance and capacitance of the PV cells, respectively, $I_s = 9 \times 10^{-11}$ A is the saturation current, R_s and R_{sh} are the series and shunt resistance of the array, respectively, i_{pv} is the current flowing through the array, v_{pv} is the output voltage of the array, N is the turns-ratio of the step-up transformer, R_{dc} is the resistance, L_{dc} is the reactance, C_{dc} is the capacitance, G is the solar irradiance, i_{dc} is the current flowing through and v_{dc} is the output voltage of the DC-link, P_{pv} is the power of the PV array which is a function of v_{dc}, G and T, and $P = 3/2(v_d i_d + v_q i_q)$ is the output power, where v_d and v_q are the direct- and quadrature-axis components of the output voltage, respectively, and i_d and i_q are the direct- and quadrature-axis components of the current, respectively.

The converter control of a solar PV system is shown in Fig. 10.7. The real and reactive power generated and absorbed by the voltage source converter (VSC) can be controlled by controlling its firing angle, α_{pv} and modulation index, m_{pv}. In this study, the reactive power, Q_{ref} is set to zero to operate the PV generator at unity pf and $Q = 3/2(v_q i_d - v_d i_q)$. A shunt AC filter is not considered in the PV model since its effect is more relevant for an electromagnetic transient analysis [27].

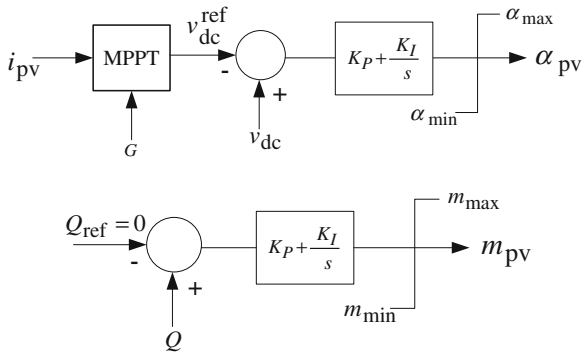

Fig. 10.7 Converter control of PV generator

10.3.2 D-STATCOM

A D-STATCOM is a shunt-connected flexible alternating current transmission system (FACTS) device that regulates the voltage of an AC bus. The regulation is done by a VSC connected to a DC capacitor, as shown in Fig. 10.8. The dynamics of this voltage source is governed by the charging and discharging of a large (nonideal) capacitor. The capacitor voltage can be adjusted by controlling the phase angle difference between line voltage, v_s and VSC voltage, E ($E = kv_{\text{dcs}}\angle\alpha$). If the phase angle of the line voltage is taken as a reference, that of the VSC voltage is the same as the firing angle, α, of the VSC. Thus, if α is slightly advanced, the DC voltage, v_{dcs}, decreases and reactive power flows into the D-STATCOM. Conversely, if α is slightly delayed, the DC voltage increases and the D-STATCOM supplies reactive power to the bus. By controlling α, the reactive power can be supplied from or absorbed by the D-STATCOM and, thus, the voltage regulation can be achieved.

The dynamics of a D-STATCOM can be described by the following equation:

$$\dot{v}_{dcs}(t) = -\frac{P_s}{C_s v_{\text{dcs}}} - \frac{v_{\text{dcs}}}{R_{cs} C_s}, \tag{10.6}$$

where v_{dcs} is the capacitor voltage, C_s is the DC capacitance, R_{cs} is the internal resistance of the capacitor, P_s is the power supplied by the system to the D-STATCOM to charge the capacitor which is a nonlinear function of (α, k, E, v_{dc}, v_d and v_q) [28].

The terminal voltage of the D-STATCOM is measured using a transducer with first-order dynamics,

$$\dot{v}_{sm} = -\frac{v_{sm}}{T_m} + K_m v_s, \tag{10.7}$$

where v_{sm} is the sensor output and v_s is the voltage at the connection point of the D-STATCOM, K_m is a constant and T_m is the time constant of the voltage transducer. In this chapter, the constant associated with the inverter, k is fixed and

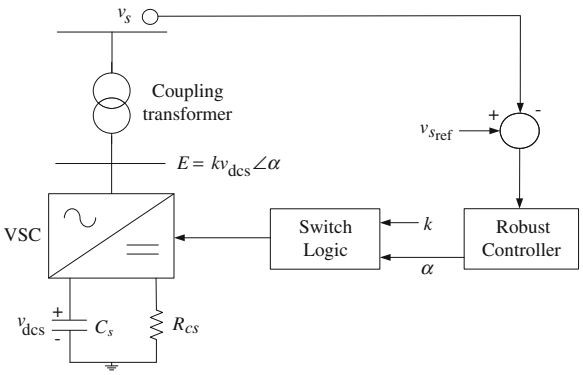

Fig. 10.8 D-STATCOM equivalent circuit with its control

the firing angle, α is used as the control variable. In the load flow, the D-STATCOM is modeled as a generator bus (PV bus) with $P_G = 0$.

10.3.3 Load

The following exponential forms are used to represent a static load.

$$P(V) = P_0\left(\frac{V}{V_0}\right)^a, \tag{10.8}$$

$$Q(V) = Q_0\left(\frac{V}{V_0}\right)^b, \tag{10.9}$$

where P and Q are the active and reactive components of the load, respectively and V is the bus voltage magnitude. The subscript 0 identifies the values of the respective variables at the initial operating condition. The parameters of this model are the exponents a and b. With these exponents equal to 0, 1 or 2, the model represents the constant power, constant current or constant impedance characteristics of load components, respectively.

For composite loads, the load components for the nominal system are aggregated assuming that a load delivery point consists of 30 % static loads (space heating, cooking, water heater, etc.), 10 % fluorescent lamps [24] and 60 % induction motors [24]. In this study, the active components of static loads are represented by constant current models and reactive components by constant impedance models, as recommended in [9] for dynamic simulations.

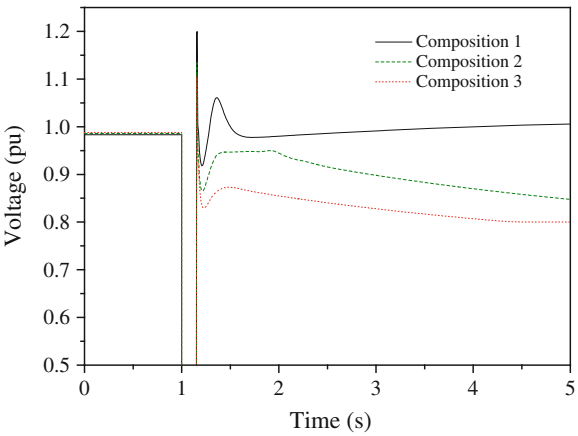

Fig. 10.9 Voltage at PCC (bus 13) for various load compositions

Table 10.5 Different load compositions in composite load model

No.	Static (%)	Fluorescent lighting (%)	Induction motor (%)
Composition 1	45	15	40
Composition 2	30	10	60
Composition 3	15	5	80

10.4 Impact of Different Load Compositions

In order to investigate the dynamic behavior of the system with the composite load model, the system is tested with a sudden three-phase short-circuit fault at bus 2 for a fault duration of 150 ms. Figure 10.9 shows the voltage at the point of common coupling (PCC) for different load compositions in Table 10.5. The figure illustrates that the composition of load has a great impact on the system stability. From Fig. 10.9, it can be seen that the system has transient over-voltage in all cases and it fails to return to pre-fault condition as the proportion of induction motors in the load composition increases. The voltage profiles at different load buses with the load composition 3 under the same disturbance are shown in Fig. 10.10. Real and reactive powers drawn by the loads in those buses are shown in Figs. 10.11 and 10.12, respectively. From Figs. 10.11 and 10.12, it can be observed that the real powers are less sensitive to the disturbance, however, dynamic loads cause voltage instability due to their high reactive power consumption after a sudden disturbance. To overcome the instability problem, the system requires dynamic compensating devices to maintain the grid code requirements in Table 10.2.

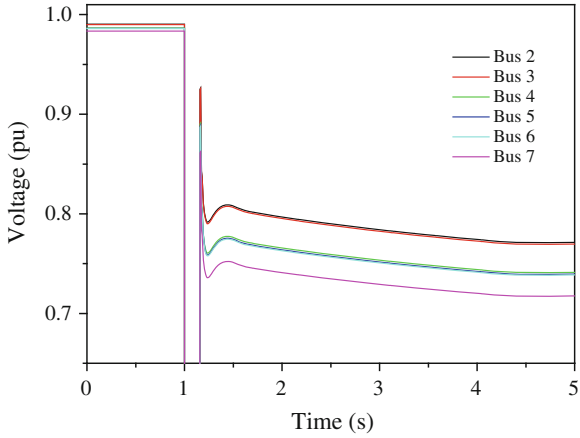

Fig. 10.10 Voltages at different load buses of system without D-STATCOM

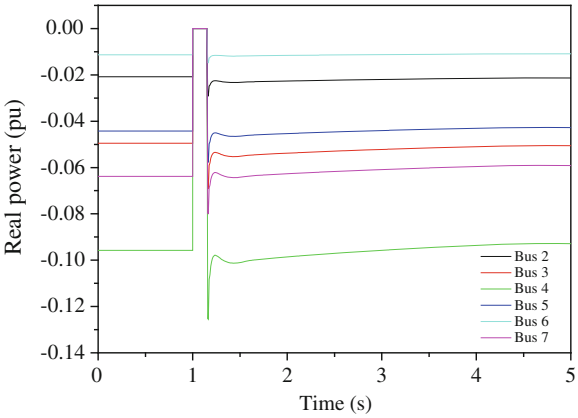

Fig. 10.11 Real power drawn by loads at different buses without D-STATCOM

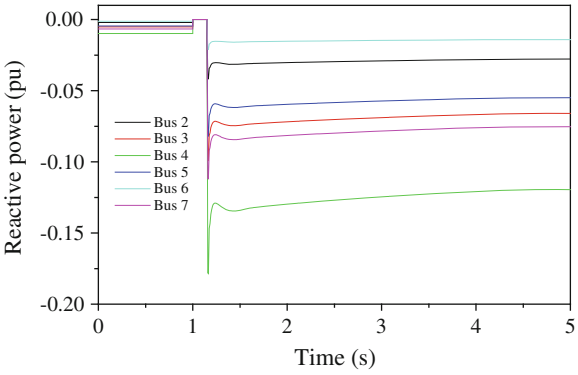

Fig. 10.12 Reactive power consumed by loads at different buses without D-STATCOM

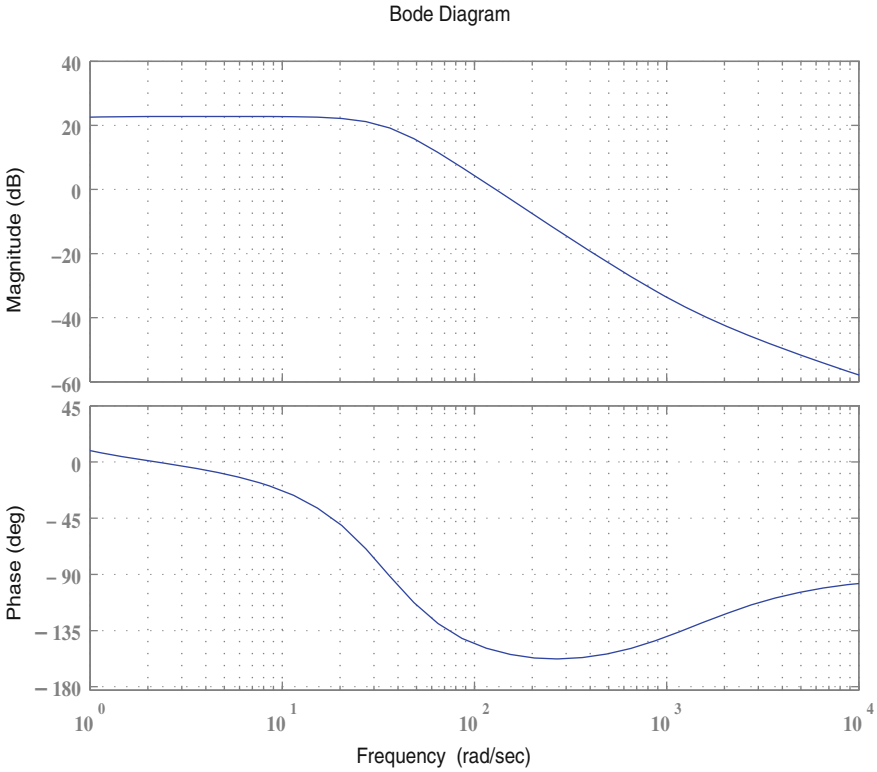

Fig. 10.13 Bode plot of open-loop system with converter control—transfer function from input (firing angle) to terminal voltage

10.5 Controller Design for D-STATCOM

The problem considered here is the design of a robust controller which works for various load compositions in the composite load. Modal analysis is performed on the grid-connected PV system to obtain an idea of the dominant mode which needs to be controlled [12]. The dominant mode of the nominal test system is monotonic with an eigenvalue at −0.00059. The normalized participation factors indicate that system voltage states ($v_{pv} = 1.0$, $v_{dc} = 0.96$, $v_{dcs} = 0.57$) have significant contributions in this mode. This marginally stable mode causes unstable operation during large disturbances in the system. The open-loop frequency response of the system with converter controller is shown in Fig. 10.13 in which it can be observed that the system has an inadequate margin (phase margin 28.55 deg) in order to withstand disturbances.

10.5.1 LQG Controller

The system to be controlled can be written as

$$\begin{aligned} \dot{x}(t) &= Ax(t) + Bu(t), \\ y(t) &= Cx(t), \end{aligned} \tag{10.10}$$

where A is the system matrix, B is the control or input matrix, C is the output matrix, $x = \left[i_{\text{pv}}, v_{\text{pv}}, i_{\text{dc}}, v_{\text{dc}}, v_{\text{dcs}}, v_{sm}\right]^T$, input, $u = \alpha$ and output, $y = v_{sm}$.

The standard LQR cost function can be defined as

$$J = \lim_{T\to\infty} \frac{1}{T} E \int_0^T \left(x^T Q_r x + u^T R_r u\right) dt, \tag{10.11}$$

where Q_r is a positive semi-definite state weighting matrix and R_r is a positive definite control weighting matrix, that is, $Q_r = Q_r^T \geq 0$, $R_r = R_r^T > 0$ and E is the expectation operator.

The controller for the nominal system that consists of a LQR and a Kalman-Bucy filter (KBF) is given by [22]

$$\dot{x}_c = A_c x_c + B_c(\Delta V_{\text{ref}} - V_{sm}), \tag{10.12}$$

$$y_c = C_c x_c, \tag{10.13}$$

where

$$A_c = A - BR_r^{-1}B^T P_r - P_f C^T R_f^{-1} C, \tag{10.14}$$

$$B_c = P_f C^T R_f^{-1}, C_c = R_r^{-1} B^T P_r. \tag{10.15}$$

The matrices P_r and P_f are symmetric positive-definite solutions of the control and filter algebraic Riccati equations given by equations (10.16) and (10.17), respectively.

$$P_r A + A^T P_r - P_r B R_r^{-1} B^T P_r + Q_r = 0, \tag{10.16}$$

$$P_f A^T + A P_f - P_f C^T R_f^{-1} C P_f + Q_f = 0. \tag{10.17}$$

For the given test system, the weighting matrices for the standard LQG controller are chosen as $Q_r = \text{diag}(1, 1, 1, 10, 15, 5)$ and $R_r = 1$ to calculate the optimal gain. As IEEE Std. 1547 [13, 14] does not allow to regulate the voltage at the PCC actively, in this chapter, the location of the D-STATCOM is determined based on the weak bus oriented D-STATCOM placement planning to increase the system's Q-margin [29]. As, according to [29], the most suitable location for the D-STATCOM in this study is bus 15, which is the most critical bus in this

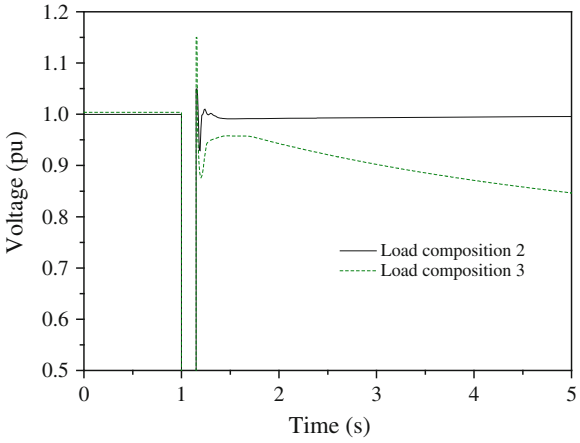

Fig. 10.14 Performances of standard LQG controller for different load compositions

network, to evaluate the performance of the designed controller, simulations are carried out on the nonlinear model of the system by connecting the D-STATCOM at bus 15.

To demonstrate the performance of the standard LQG controller [30], the voltage profile of the system with the controller is shown in Fig. 10.14 for a sudden three-phase short-circuit fault of 150 ms at bus 2. From Fig. 10.14, it can be seen that the standard LQG controller performs well to recover the voltage within the utility's time frame for the nominal system load composition. As the standard LQG controller is designed for the nominal system (with load composition 2), it can ensure the performance for the plant for which it is designed. However, it cannot provide robust performance when the load composition changes (load composition 3), as depicted in Fig. 10.14. The results of stability simulations indicate that the performance of the controller can be drastically affected by the variations in load compositions which motivates the design of a robust controller for the D-STATCOM.

10.5.2 Norm-Bounded LQG Controller

To facilitate the control design, the uncertain system can be represented as

$$\begin{aligned} \dot{x}(t) &= A(p)x(t) + B(p)u(t), \\ y(t) &= C(p)x(t), \end{aligned} \tag{10.18}$$

where $p \in \mathbb{R}^k$ denotes the vector of uncertain parameters; $A(p), B(p), C(p)$ are appropriately dimensioned matrices assumed to be affine functions of the parameter vector, p. The parameters $p_i, i = 1, 2, \ldots, k$, which are components of p,

are assumed to lie in a convex polytopic region ζ in the parameter space, bounded by vertices $p^j, j = 1, 2, \ldots, l$.

During the design procedure of the controller, the system with load composition 2 is considered as the nominal system. The first step in the design of robust controller using the proposed method is to linearize the system in the region given by the nominal load, p_0 and changes in the system model due to variations in load compositions, Δp. From the simulations of the variations in load compositions, we obtain p, which is made up of the end-points of the region of interest. $A(p)$ is calculated for all possible combinations of these quantities. The corner points for $A(P)$ are given by $\bar{P}_{ls} = P_{ls0} + 0.15\,\text{pu}$, $\underline{P}_{ls} = P_{ls0} - 0.15\,\text{pu}$; $\bar{Q}_{ls} = Q_{ls0} + 0.15\,\text{pu}$, $\underline{Q}_{ls} = Q_{ls0} - 0.15\,\text{pu}$; $\bar{P}_{lf} = P_{lf0} + 0.05\,\text{pu}$, $\underline{P}_{lf} = P_{lf0} - 0.05\,\text{pu}$; $\bar{Q}_{lf} = Q_{lf0} + 0.05\,\text{pu}$, $\underline{Q}_{lf} = Q_{lf0} - 0.05\,\text{pu}$; $\bar{P}_{lm} = P_{lm0} + 0.20\,\text{pu}$, $\underline{P}_{lm} = P_{lm0} - 0.20\,\text{pu}$; $\bar{Q}_{lm} = Q_{lm0} + 0.20\,\text{pu}$, $\underline{Q}_{lm} = Q_{lm0} - 0.20\,\text{pu}$, where P_{ls} and Q_{ls} are the real and reactive power of static loads, respectively, P_{lf} and Q_{lf} are the real and reactive power of fluorescent lighting loads, respectively, and P_{lm} and Q_{lm} are the real and reactive power of induction motors, respectively, in the aggregated model.

In this study, the power supplied by the system, P_s, to the D-STATCOM to charge the capacitor is a nonlinear function of the control input, α. Considering 10 % uncertainty in the input, corner points for $B(P)$ are given by $\bar{P}_s = P_{s0} + 0.1\text{pu}$, $\underline{P}_s = P_{s0} - 0.1\text{pu}$.

The output matrix C is defined as $C = [0, 0, 0, 0, 0, 1]$. Considering 5 % uncertainty due to the measurement error in the output, the corner points for $C(p)$ are given by $\bar{V}_s = V_{s0} + 0.05\text{pu}, \underline{V}_s = V_{s0} - 0.05\,\text{pu}$.

The problem is to obtain a controller which minimizes the performance function (10.11) under the constraint (10.18). The approach considered here is to find the smallest upper bound on the H_∞ norm of the uncertain system and then an optimal controller is designed with this bound.

Suppose that there is a positive-definite symmetric matrix P and a scalar $\sigma > 0$ such that [22]

$$Z(p^j, P) := \begin{bmatrix} A(p^j)^T P + PA(P^j) + C(p^j)^T C(p^j) & PB(p^j) \\ \mathrm{B}(p^j)^T P & -\sigma I \end{bmatrix} \leq 0, \qquad (10.19)$$

for $j = 1, 2, \ldots, l$.

To find the smallest upper bound on $G(p^j, s) = C(p^j)[sI - A(p^j)]^{-1}B(p^j)$, it is necessary to minimize σ.

If the inequality (10.19) is satisfied for all p^j then,

$$\| G(p^j, s) \|_\infty \leq \gamma := \sqrt{\sigma}, \forall p \in \zeta$$

For the nominal system (A, B, C), $\| G(s) \|_\infty \leq \gamma$, iff there is a symmetric positive-definite matrix P such that the following inequality is satisfied.

$$\begin{bmatrix} A^T P + PA + C^T C & PB \\ B^T P & -\gamma^2 I \end{bmatrix} \leq 0. \qquad (10.20)$$

The problem is to find an LQG controller whose infinity norm is bounded by a given number μ [22],

$$\| \mathrm{G_c(s)} \|_\infty \leq \mu, \text{such that } 0 < \mu < 1/\gamma,$$

where $G_c(s) = C_c(sI - A_c)^{-1}B_c$.

Without loss of generality (Appendix-II), to reduce computational complexity, an equivalent condition (10.25) is derived which is in the form of inequality (10.20) with $P = I$ and the resulting transformed system takes the form of equation (10.24).

Suppose that [22] the LQG performance function weights are such that $Q_r > 0$ and

$$R_r \geq I, \tag{10.21}$$

$$Q_r > \mu^{-2} P_r \hat{C}^T R_f^{-2} \hat{C} P_r - \hat{C}^T R_f^{-1} \hat{C} P_r - P_r \hat{C}^T R_f^{-1} \hat{C}, \tag{10.22}$$

$$Q_f = -\left(\hat{A} + \hat{A}^T\right) + \hat{C}^T R_f^{-1} \hat{C}. \tag{10.23}$$

Then, the controller is norm bounded by μ $(0 < \mu < \frac{1}{\gamma})$, if (10.21)–(10.23) are satisfied.

10.5.3 Design Steps

The design steps of the LQG optimal norm-bounded controller for the nominal system are given below:

Step 1: Obtain the region of interest by varying load compositions in the composite load.

Step 2: Find the smallest upper bound γ on the norm of the uncertain system so that the inequality (10.19) is satisfied.

Step 3: Obtain a solution P to the linear matrix inequality (10.20) for the nominal system and transform the system matrices using the similarity transformation, $z = \Gamma x$.

Step 4: Choose the LQR weighting matrices $R_r \geq I$ and $Q_r > 0$ based on the performance requirements and choose the scalar μ, $0 < \mu < \frac{1}{\gamma}$.

Step 5: Solve equation (10.16) for P_r and choose R_f such that (10.22) is satisfied.

Using the above steps, the required controller is given by equations (10.14) and (10.15) with $P_f = I$.

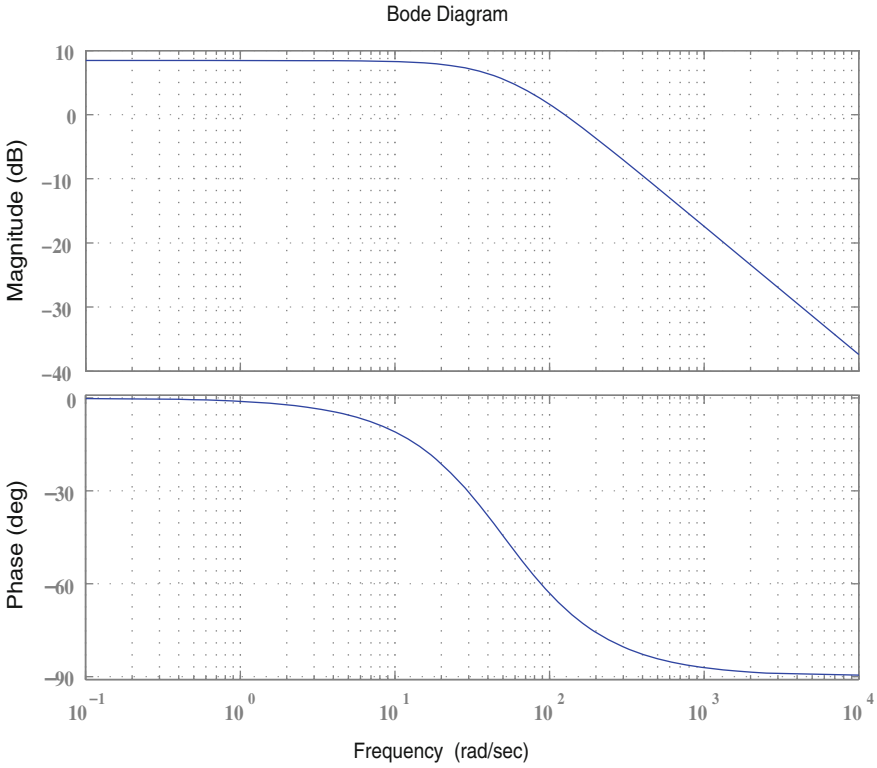

Fig. 10.15 Bode plot of robust D-STATCOM controller—firing angle versus terminal voltage

10.6 Performance Evaluation

In order to improve the system's performance under varying operating conditions, a robust LQG controller is designed according to the Steps 1–5 described in Subsection 10.5.3. For the proposed approach, the smallest H_∞ norm-bound is found to be $\gamma = 1.15$. A norm-bounded controller is designed to have an H_∞ norm less than $1/\gamma$. The weighting matrices are chosen as

$$Q_r = \text{diag}(1, 1, 1, 12, 20, 10), R_r = 1.5, R_f = 1.$$

Q_r and R_r are chosen so as to give good regulator performance and R_f is chosen so as to satisfy (10.22). There is a considerable freedom in choosing the regulator weighting matrices Q_r and R_r, but limited freedom in choosing the filter weighting matrices Q_f and R_f. This is to be expected because the objective is to limit the overall controller gain which consists of the product of the LQR and KBF gains. A suitable balance between the LQR and KBF gains can be obtained by adjusting Q_r and R_r in such a way as to permit a smaller R_f [22].

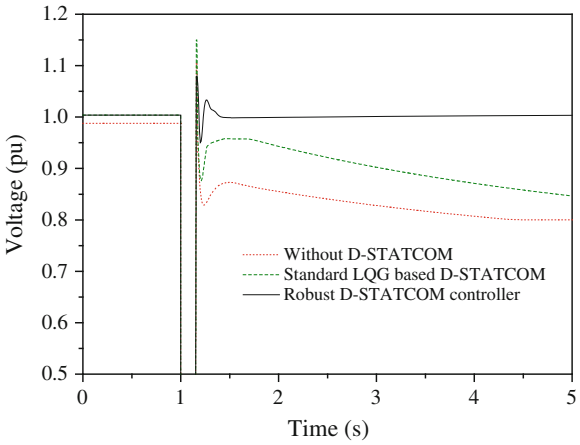

Fig. 10.16 Voltage at PCC (bus 13) for load composition 3 (80 % induction motor in composite load model)

The frequency response of the proposed controller in Fig. 10.15 signifies that it provides adequate bandwidth and margins to stabilize the system under different operating conditions. The closed-loop eigenvalue of the dominant mode is found at −4.512. To examine the robustness of the proposed controller, the following contingencies are applied:

- a symmetrical three-phase short-circuit fault close to the substation; and
- an asymmetrical fault close to the DG unit.

10.6.1 Contingency I: Three-Phase Short-Circuit Fault Close to Substation

In the studies of cases involving a short-circuit fault, the load characteristics during a fault might deserve far more attention as bus voltages are depressed and eventually affect the stability of the system. In the demonstrated test system, main source of reactive power support to the load is the substation located at bus 1. To test the controller performance under a severe disturbance, the system is operated with the load composition 3 and a three-phase short-circuit fault is applied near the substation at bus 2 for 150 ms. From Fig. 10.16, it can be observed that although the standard LQG controller fails to operate for a change in the load composition, the proposed H_∞ norm-bounded LQG controller provides the grid code-compatible performance due to the incorporation of load uncertainties in the design process. It can be also observed from Fig. 10.16 that the system with the robust D-STATCOM causes less transient over-voltage than the case without a D-STATCOM. Voltages at the different load buses under the same disturbance

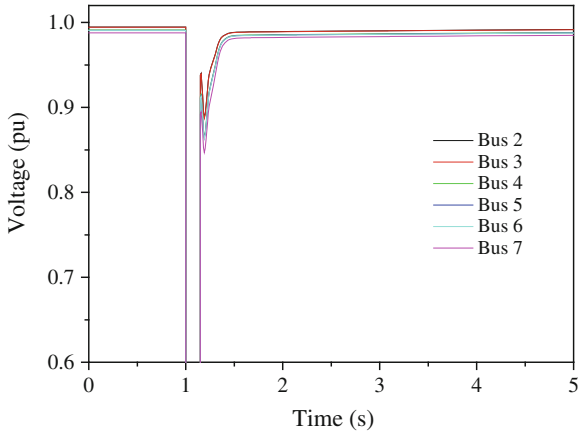

Fig. 10.17 Voltages at different load buses of system with robust D-STATCOM

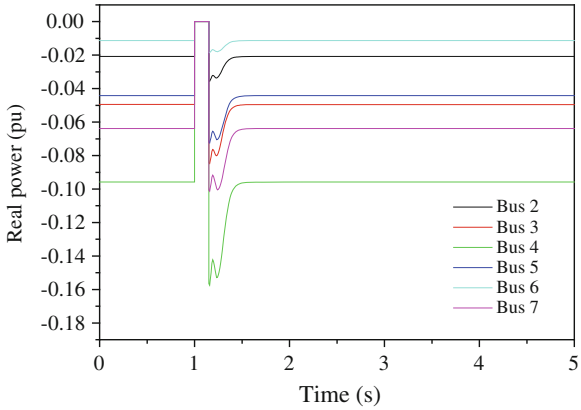

Fig. 10.18 Real power drawn by loads at different buses with robust D-STATCOM

with the proposed control scheme can be seen from Fig. 10.17. Real and reactive power drawn by the load before, during and after the disturbance are given in Figs. 10.18 and 10.19, respectively. In all cases, the system returns to pre-fault condition within a short-time. The outputs from the D-STATCOM for the standard LQG and robust LQG controller are shown in Fig. 10.20 in which it can be observed that the robust LQG controller supports reactive power to the system instantaneously following a disturbance, thereby improving voltage performance. The results obtained for the fault condition reveal superior dynamic performance and fast fault recovery of the designed D-STATCOM.

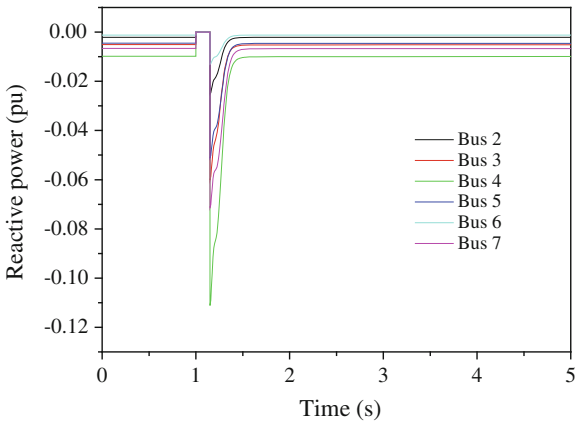

Fig. 10.19 Reactive power consumed by loads at different buses with robust D-STATCOM

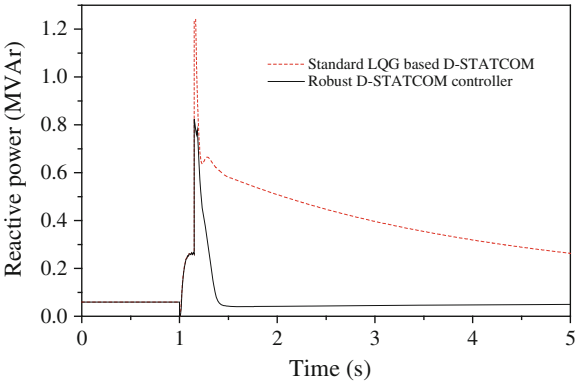

Fig. 10.20 Reactive power output of D-STATCOM (sudden three-phase fault at bus 2)

10.6.2 Contingency II: Asymmetrical Fault Close to DG Unit

To observe the effect of an unbalanced fault, a single-line-to-ground fault is applied in the middle of the line connecting the buses 12 and 13. In this case, the system is operated with 70 % induction motor loads, 10 % fluorescent lamps and 20 % static loads in the composite load model. The fault is applied at 1 s and cleared after 150 ms. The voltage profile of the system at the PCC is shown in Fig. 10.21. It can be investigated form Fig. 10.21 that although the controller is designed for the nominal system, it performs well for a variation in the system model and the original system is restored after the clearance of the fault. Reactive power consumed by the load at bus 12 is shown in Fig. 10.22. The robust D-STATCOM

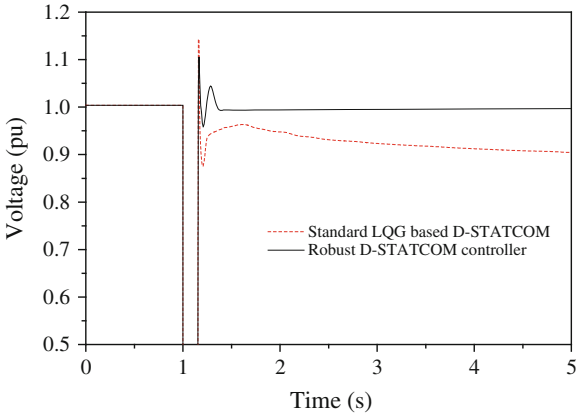

Fig. 10.21 Voltage at PCC (bus 13) for asymmetrical fault (70 % induction motor in composite load model)

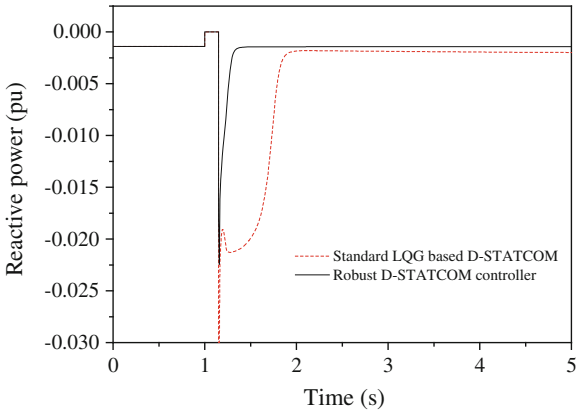

Fig. 10.22 Reactive power consumed by load at bus 12

injects reactive power to the load following a disturbance and the system voltage starts to recover. The applied control effort α by the designed controller to stabilize the system can be observed in Fig. 10.23.

The above investigations demonstrate that the proposed controller is robust against changes in operating conditions and stabilizes the system under large disturbances to ensure DG units remain connected to the network.

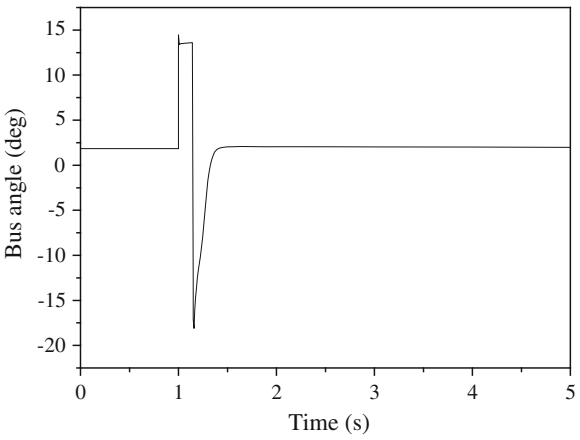

Fig. 10.23 Control effort (α) with designed controller for single-line-to-ground fault in middle of line 12−13

Table 10.6 PV system data

Number of PV cells per module	54
Number of parallel modules in each row	150
Module current rating	2.8735 A
Module voltage rating	43.5 V
Voltage temperature coefficient	−0.1 V/K
Current temperature coefficient	0.003 A/K
Diode ideality factor	1.3
VSC switching frequency	3060 Hz
On-state resistance of VSC valves	1 mΩ
Solar irradiance, G	1.0 kW/m^2
Series resistance, R_s	0.0819 Ω
Shunt resistance, R_{sh}	72 kΩ
PV inductance, L_{pv}	1.0 μH
PV capacitance, C_{pv}	10 mF
DC-link resistance, R_{dc}	0.1 Ω
DC-link inductance, L_{dc}	1.0 mH
DC-link capacitance, C_{dc}	400 μF
Transformer ratio, N	15

Table 10.7 Line and load data of 16-bus distribution system

SE	RE	R (pu)	X (pu)	P_l (pu)	Q_l (pu)	C (pu)
1	8	0.110	0.110	0.040	0.027	0.000
8	9	0.080	0.110	0.050	0.030	0.012
8	10	0.110	0.110	0.010	0.009	0.000
9	11	0.110	0.110	0.006	0.001	0.006
9	12	0.080	0.110	0.045	0.020	0.037
2	4	0.075	0.110	0.020	0.016	0.000
4	5	0.080	0.110	0.030	0.015	0.011
4	6	0.090	0.180	0.020	0.008	0.012
6	7	0.040	0.040	0.015	0.012	0.000
3	13	0.110	0.110	0.010	0.009	0.000
13	14	0.090	0.120	0.010	0.007	0.018
13	15	0.080	0.110	0.010	0.009	0.000
15	16	0.040	0.040	0.021	0.010	0.018
5	11	0.040	0.040	0.000	0.000	0.000
10	14	0.040	0.040	0.000	0.000	0.000

(Base power is 100 MVA and base voltage is 23 kV, SE and RE are the sending and receiving end nodes, respectively)

Table 10.8 Line and load data of 15-bus Kumamoto distribution system

SE	RE	R (pu)	X (pu)	B (pu)	P_l (pu)	Q_l (pu)
1	2	0.003145	0.075207	0.00000	0.02080	0.0021
2	3	0.000330	0.001849	0.00150	0.04950	0.0051
3	4	0.006667	0.030808	0.03525	0.09580	0.0098
4	5	0.005785	0.014949	0.00250	0.04420	0.0045
5	6	0.014141	0.036547	0.00000	0.01130	0.0012
4	7	0.008001	0.036961	0.03120	0.06380	0.0066
7	8	0.008999	0.041575	0.00000	0.03230	0.0033
8	9	0.007000	0.032346	0.00150	0.02130	0.0022
9	10	0.003666	0.016940	0.00350	0.02800	0.0029
10	11	0.008999	0.041575	0.00200	0.21700	0.0022
3	12	0.027502	0.127043	0.00000	0.01320	0.0014
12	13	0.031497	0.081405	0.00000	0.00290	0.0003
13	14	0.039653	0.102984	0.00000	0.01610	0.0016
14	15	0.016070	0.004153	0.00000	0.01390	0.0014

(Base power is 10 MVA and base voltage is 6.6 kV, SE and RE are the sending and receiving end nodes, respectively.)

10.7 Conclusions

In this chapter, the impacts of solar PV generators and composite loads on distribution systems are analyzed and a novel control methodology is proposed to ensure grid code-compatible performances of PV generators connected to distribution networks. Static analyses show that the loss of multiple solar PV generators,

overloading and line outages from a distribution network can be a risk for the system stability. Dynamic analyses illustrate that the proportion of induction motor load in the composite load model has a significant impact on the stability of a distribution network. It is investigated that a high percentage of induction motors in the composite load model affects the dynamic voltage stability of the system. A novel controller for a D-STATCOM is proposed to solve this problem. The proposed control scheme determines the smallest upper bound on the H_∞ norm of the uncertain system. The effectiveness of the proposed controller is verified through time-domain simulation studies conducted on a widely used test system. The results show that the distributed PV system with the proposed robust D-STATCOM controller maintains its stability despite major variations in load compositions. As, in a practical system, there are always continual variations in the load compositions itself, the proposed control method provides a good reflection of the reality for supporting DG integration.

Appendix-I

The data of the PV system is given in Table 10.6. D-STATCOM parameters: 1.0 MVA, C_s= 300 μF, R_{cs}= 0.01 pu. The data of 16-bus and 15-bus distribution test systems are given in Table 10.7 and Table 10.8, respectively.

Appendix-II

Suppose that $\Gamma \in \mathbb{R}^{n\times n}$ is a square root of P, i. e., $P = \Gamma^T\Gamma$. Using the coordinate transformation ($\xi = \Gamma x$), the system becomes

$$\dot{\xi} = \hat{A}\xi + \hat{B}u, \qquad \mathrm{y} = \hat{C}\xi, \tag{10.24}$$

where $\hat{A} = \Gamma A\Gamma^{-1}, \hat{B} = \Gamma B, \hat{C} = C\Gamma^{-1}$.

Pre-multiplying (10.20) by $diag[\Gamma^{-T}, I]$ and post-multiplying it by its transpose, we have [22]

$$\begin{bmatrix} \hat{A}^T + \hat{A} + \hat{C}^T\hat{C} & \hat{B} \\ \hat{B}^T & -\gamma^2 I \end{bmatrix} := -\begin{bmatrix} Q_A & Q_{12} \\ Q_{12}^T & R \end{bmatrix} \leq 0. \tag{10.25}$$

Therefore, without loss of generality, it is assumed that the system is in this form [i.e., it satisfies the inequality (10.20) with $P = I$].

References

1. Renewable Energy Policy Network for 21st Century, Renewables 2010 global status report. http://www.ren21.net. Accessed 22 June 2013
2. Sengupta M, Keller J (2012) PV ramping in a distributed generation environment: a study using solar measurements. In: IEEE Photovolt Spec Conf pp 586–589
3. Schauder C (2011) Impact of FERC 661-A and IEEE 1547 on photovoltaic inverter design. In: IEEE PES General Meeting pp 1–6
4. Molina MG, Mercado PE (2008) Modeling and control of grid-connected photovoltaic energy conversion system used as a dispersed generator. In: IEEE/PES Transmission and Distribution Conference and Exposition: Latin America, pp 1–8
5. Tan YT, Kirschen DS, Jenkins N (2004) A model of PV generation suitable for stability analysis. IEEE Trans Energy Convers 19(4):748–755
6. Rodriguez C, Amaratunga GAJ (2004) Dynamic stability of grid-connected photovoltaic systems.In: IEEE Power Engineering Society General Meeting pp 2193–2199
7. Eltawil MA, Zhao Z (2010) Grid-connected photovoltaic power systems: technical and potential problems—a review. Renew Sustain Energy Rev 14(1):112–129
8. Atwa YM, El-Saadany EF (2009) Reliability evaluation for distribution system with renewable distributed generation during islanded mode of operation. IEEE Trans Power Systems 24(2):572–581
9. IEEE Task Force (1993) Load representation for dynamic performance analysis. IEEE Trans on Power Systems 8(2):472–482
10. Concordia C, Ihara S (1982) Load representation in power system stability studies. IEEE Trans Power Apparatus Syst PAS-101(4): 969–977
11. Roy NK, Hossain MJ, Pota HR (2011) Effects of load modeling in power distribution system with distributed wind generation.In: 21st Australasian Universities Power Engineering Conference pp 1–6
12. Kundur P (1994) Power system stability and control. McGraw-Hill, New York
13. IEEE Std. 1547 (2003) IEEE standard for interconnecting distributed resources with electric power systems
14. IEEE Std 1547.2 (2008) IEEE application guide for IEEE Std 1547, IEEE standard for interconnecting distributed resources with electric power systems
15. Mahmud MA, Pota HR, Hossain MJ, Roy NK (2014) Robust partial feedback linearizing stabilization scheme for three-phase grid-connected photovoltaic systems. IEEE J Photovolt 4(1): 423–431
16. IEEE Power and Energy Series—Song YH, Johns AT(eds) (1999) Flexible AC transmission systems (FACTS). The Institution of Electrical Engineers, London
17. Hingorani NG, Gyugyi L (2000) Understanding FACTS-concepts and technology of flexible AC transmission systems. IEEE Press, New York
18. Yunus AMS, Masoum MAS, Abu-Siada A (2011) Effect of STATCOM on the low-voltage ride-through capability of Type-D wind turbine generator. In: Innovative Smart Grid Technologies Asia pp 1–5
19. Yang K, Cheng X, Wang Y et al (2012) PCC voltage stabilization by D-STATCOM with direct grid voltage control strategy. In: Innovative Smart Grid Technologies Asia pp 1–5
20. Rao P, Crow ML, Yang Z (2000) STATCOM control for power system voltage control applications. IEEE Trans Power Delivery 15(4):1311–1317
21. Seo JC, Kim TH, Park JK , Moon SI (1996) An LQG based PSS design for controlling the SSR in power systems with series-compensated lines. IEEE Trans Energy Conversion 11(2):423–428
22. Joshi SM, Kelkar AG (2002) Design of norm-bounded and sector-bounded LQG controllers for uncertain systems. J Optim Theory Appl 113(2):269–282
23. Civanlar S, Grainger JJ, Yin H , Lee SSH (1988) Distribution feeder reconfiguration for loss reduction. IEEE Trans Power Delivery 3(3):1217–1223

24. Taylor CW (1994) Power system voltage stability. McGraw-Hill, New York
25. Li S, Tomsovic K, Hiyama T (2000) Load following functions using distributed energy resources. In: IEEE Power Engineering Society Summer Meeting pp 1756–1761
26. Hossain MJ, Saha TK, Mithulananthan N, Pota HR (2012) Robust control strategy for PV system integration in distribution systems. Appl Energy 99:355–362
27. Milano F (2010) Power system modeling and scripting. Springer-Verlag, London
28. Hossain MJ, Pota HR, Ramos RA (2011) Robust STATCOM control for the stabilisation of fixed-speed wind turbines during low voltages. Renewable Energy 36(11):2897–2905
29. Roy NK, Pota HR, Hossain MJ (2013) Reactive power management of distribution networks with wind generation for improving voltage stability. Renewable Energy 58:85–94
30. Anderson BDO, Moore JB (1990) Optimal control: linear quadratic methods. Prentice-Hall, New Jersey